



Synthesis and characterization of Sn doped TiO₂ photocatalysts: Effect of Sn concentration on the textural properties and on the photocatalytic degradation of 2,4-dichlorophenoxyacetic acid



I. Rangel-Vázquez^a, G. Del Angel^{a,*}, V. Bertin^a, F. González^b, A. Vázquez-Zavala^a, A. Arrieta^a, J.M. Padilla^c, A. Barrera^d, E. Ramos-Ramírez^e

^aDepartamento de Química, Universidad Autónoma Metropolitana-Iztapalapa, Av. San Rafael, Atlixco No 1865, México 09340 D.F., Mexico

^bDepartamento de Ingeniería de Procesos e Hidráulica, Universidad Autónoma Metropolitana-Iztapalapa, Av. San Rafael, Atlixco No 1865, México 09340 D.F., Mexico

^cUniversidad Tecnológica del Centro de Veracruz, Área de Tecnología, Av. Universidad Carretera Federal Cuitláhuac-La Tinaja No. 350, Cuitláhuac, Veracruz 94910, Mexico

^dUniversidad de Guadalajara, Centro Universitario de la Ciénega, Av. Universidad, Número 1115, Col. Linda Vista, Apdo. Postal 106, Ocotlán Jal., Mexico

^eDepartamento de Química, División de Ciencias Naturales y Exactas, Campus Guanajuato de la Universidad de Guanajuato Noria Alta S/N, Col. Noria Alta, Guanajuato, Gto. C.P. 36050, Mexico

ARTICLE INFO

Article history:

Available online 23 December 2014

Keywords:

TiO₂-SnO₂
Rietveld refinement
Sol-gel synthesis
Semiconductor
2,4-D photodegradation

ABSTRACT

TiO₂ and Sn-doped TiO₂ materials were prepared by sol-gel method using titanium and tin alkoxides at different Sn concentration (0.1 mol%, 0.5 mol%, 1 mol%, 3 mol% and 5 mol%). Samples were characterized by thermo gravimetric analyzer with differential scanning calorimeter (TGA-DSC), X-ray Rietveld refinement, N₂ adsorption (BET), transmission electron microscopy (TEM), UV-vis spectroscopies technology and Raman spectroscopy. Only anatase phase was observed in pure TiO₂, whereas anatase and brookite were obtained in Sn-doped TiO₂ samples. Sn dopant acts as a promoter in phase transformation of TiO₂. The Rietveld refinements method was used to determine the relative weight of anatase and brookite, and crystallite size as a function of Sn concentration after calcination of samples at 673 K. It was also demonstrated the incorporation of Sn⁴⁺ into the anatase TiO₂ structure. Sn⁴⁺ inhibits the growth of TiO₂ crystallite size, which leads to an increase of the specific surface area of TiO₂. From XRD analysis, the solid solution limit of Sn⁴⁺ into TiO₂ is 5 mol% Sn. The photocatalytic activity on Sn⁴⁺ doped TiO₂ was determined for the 2,4-dichlorophenoxyacetic acid reaction. The maximum in activity was attributed to the coexistence of anatase and brookite phases in the appropriate ratio and crystallite size.

© 2015 Elsevier B.V. All rights reserved.

1. Introduction

Titanium dioxide (TiO₂) is an n-type semiconductor, which can be found in any of its three polymorphs: anatase, brookite, and rutile. TiO₂ is widely used in various scientific and technological fields due to properties such as non-toxicity, chemical stability, low cost and optical properties. All these TiO₂ properties can be applied in different areas of research such as: development of solar cells [1], production of sensors [2], thin films [3], hydrogen production and photocatalysis [4]. However, the use of TiO₂ in photocatalytic process exhibits a rapid recombination of the electron-hole after the photo excitation of TiO₂, which leads to a decrease in the photodegradation activity of recalcitrant organic compounds. Some alternatives that improve the above-mentioned problem consist in the modification of TiO₂ by metal doping using Ce [5],

Sn [3,6,7], Nd [8], Sc and V [9], non-metal doping using N [10,11], C [12], S [13], B [14] and also co-doping with C-N [15], S-Gd [16] and Gd, N, C, and P quaternary doped-TiO₂ [4]. Likewise, coupling with another metal oxide such as Fe₂O₃, WO₃, ZnO, SnO₂ and the incorporation of precious metals generate the desired effect [17]. The TiO₂ photocatalytic properties improvement can also be achieved by doping with SnO₂. This oxide has a very important role in photocatalytic applications since it contributes to a significant increase in the production of hydroxyl radicals [6], which impact on the photocatalytic activity. Another point in favor of doping with SnO₂ is that the ionic radii of Sn⁴⁺ and Ti⁴⁺ are very similar (0.690 Å and 0.605 Å, respectively), which means that Ti⁴⁺ can be replaced by Sn⁴⁺ in the crystal structure of TiO₂ [18,19]. In the literature several methods of synthesis are reported for Sn⁴⁺ doped TiO₂ using several precursors, i.e.: the PCVD (plasma-enhanced chemical vapor deposition) method (which uses TiCl₄ and SnCl₄ for thin films formation [20]), sol-gel method (for

* Corresponding author.

the production of thin films using different precursors such as titanium (IV)-*n*-butoxide and tin (II) ethyl hexanate [6], titanium (IV) isopropoxide and SnCl₄·5H₂O [7]), and also hydrothermal [21] and co-precipitation methods. However, the sol–gel method presents significant advantages, which include the synthesis of materials at low temperatures, low cost, and the formation of materials with an arrangement clearly defined that can be controlled by the type of precursors used. Many variables can directly influence on the final properties of the synthesized material such as the addition of surfactants, the type of solvent, the acidity or basicity of the medium and the amount of water added. This paper intends to determine the effect on the structural properties of TiO₂ due to the substitution of Ti⁴⁺ by Sn⁴⁺ ions. TiO₂ samples, were synthesized by the sol–gel method, using titanium (IV) isopropoxide and tin (IV) tert-butoxide as precursors. Additional characterization, includes the study of the influence of the Sn⁴⁺ concentration in the TiO₂–SnO₂ series photocatalysts for the 2,4-dichlorophenoxyacetic acid degradation.

2. Experimental

2.1. Synthesis of TiO₂ and Sn doped TiO₂

TiO₂ and Sn-doped-titania (TiO₂–SnO₂) materials were synthesized by the sol–gel method. 87 mL of titanium (IV) isopropoxide 98+% (Strem Chemicals) were added to the required amount of tin (IV) tert-butoxide 99% (Aldrich) to have contents of 0.1, 0.5, 1, 3 and 5 mol% of tin. Finally, nitric acid (HNO₃) was added to maintain pH around 3 under solution stirring with a reflux at 343 K during 24 h. A mixture of alcohol/water (16:8 ratio) was dropwise added to the solution under vigorous stirring during 4 h and then left in reflux at 343 K for 24 h. The resultant solid was dried in an oven at 393 K for 12 h. Samples were calcined in air at 673 K for 4 h with a heating ramp of 2 K/min. Pure TiO₂ sample was prepared using the same procedure but without tin precursor. The samples were labeled as T for TiO₂ and SnXT for Sn doped TiO₂ samples, where X, is the mol% of tin.

2.2. Characterization

Thermal analysis was performed on a Thermo Gravimetric Analyser with Differential Scanning Calorimeter (TGA–DSC) TA instruments SDT-Q600 with a heating rate of 10 K/min and air flow of 60 mL/min.

The X-ray diffractograms of the powders were measured at room temperature using a Bruker D-8 Advance diffractometer with the Bragg–Brentano θ – θ geometry, Cu K α radiation, a Ni 0.5% Cu K β filter in the secondary beam, and a one-dimensional position-sensitive silicon strip detector. The diffraction intensity as a function of 2θ angle was measured between 20° and 100°, with a 2θ step of 0.020415°, for 96 s per point. Crystalline structures were refined using the Rietveld method by using a fundamental parameter approach during the refinements, as implemented in the TOPAS code, version 4.2.

The specific surface area of the samples was measured using the BET method with nitrogen as adsorbent gas and BJH method was used to obtain the pore size distribution. The samples were outgassed for 2 h with vacuum to 573 K in a Quantachrome Autosorb-3B equipment.

Raman spectra were recorded in the range of 100–3500 cm⁻¹ using an XRD Thermo Scientific Raman Microscope equipped with a Nd:YVO₄DPSS laser source. Excitation laser line was at 532 nm and the laser power of 10 mW.

TEM study was performed on an electron microscope of field emission 2010FEJ JEM that operates at 200 kV. The microscope is equipped with a field of Schottky type emission cannon and a configuration of ultrahigh resolution (UHR) (Cs = 0.5 mm; Cc 1.1 mm; point to point resolution, 0.19 nm). Samples were powdered in an agate mortar, put in a syringe were vacuum was produced and an aerosol was formed and deposited on a carbon covered copper grid. The powder was stucked on the grid by electrostatic. This method was used to avoid changes on the structure of the material.

The average size of the particle (d_s) for T and Sn1T materials was calculated using the following equation. $d_s = \frac{\sum n_i d_i^3}{\sum n_i d_i^2}$, where d_i is the diameter measured directly from the TEM micrograph and n_i is the number of particles having d_i diameter. This analysis was done using the Gatan software and counting at least 150 particles to have a good approximation of the average particle size. Energy band gap (E_g) was determined using Kubelka–Munk theory, this analysis was carried out through the diffuse reflectance spectra using a spectrophotometer Varian model mark Cary 100 equipped with an integrating sphere. The evolution of the total organic carbon (TOC) during the evaluation of photocatalytic reaction was followed using a TOC Analyzer Shimadzu 5000.

Photocatalytic degradation of 2,4-D (2,4-dichlorophenoxyacetic acid) was performed using a light Pen-Ray UV lamp (UVP products, intensity of 4400 μ W/cm² at 254 nm). The lamp is placed inside a quartz tube and consecutively is tucked inside a homemade reactor which contains 200 mL with 40 ppm of 2,4-D molecule test and 200 mg of photocatalyst at room temperature. The suspension in the absence of the light source is bubbled with dry air flow (60 mL/min) for 1 h to achieve an adsorption–desorption equilibrium between the photocatalyst surface and the pollutant. Subsequently the suspension is irradiated with UV light for 3 h. Aliquots of 3 mL were taken every 15 min. The photodegradation rate was determined using a UV–Vis spectrophotometer Agilent Technologies, model Cary 60, by following the main band of 2,4-D at 282 nm absorption.

3. Results and discussion

TGA/DSC curves of TiO₂ (T) and TiO₂-doped with 1 and 5 mol% of tin (Sn1T and Sn5T) are shown in Fig. 1, for T, Sn1T and Sn5T samples. The weight loss for all processes, endothermic and exothermic is approximately 13%, 17% and 29% respectively with respect to the original value. The loss weight occurred gradually to around 773 K. All samples showed two endothermic peaks, in the temperatures ranges of 300–500 K, 300–470 K and 300–470 K for the respective catalysts, these correspond to the elimination of the residual alcohol and water. Also, three exothermic peaks were observed for all samples. For the T sample the exothermic peaks are at temperatures of 547 K, 650 K and 737 K, in Sn1T sample these peaks are at 509 K, 640 K and 732 K and for Sn5T at 511 K, 647 K and 727 K. The first one correspond to volatilization and oxidation of the organic matter present in the xerogel, the second one to the elimination of hydroxyl groups [22] and/or to the transition of amorphous material to anatase phase [23] and the third peak corresponds to the transition from anatase to rutile phase [24]. The continuous weight loss observed in the TiO₂ and TiO₂ doped samples is characteristic of the homogeneous materials obtained by sol–gel method, and correspond to the elimination of the structural hydroxyl groups [25]. The SnO₂ synthesis by sol–gel and the TGA/DSC analysis was done in order to determine the phase crystallization of SnO₂ (graphic not included). The analysis shows an exothermic peak at 608 K and no weight loss with the increase of temperature was observed, which is attributed to the crystallization of SnO₂ [24].

The SnO₂ incorporation to TiO₂ leads to a decrease in the crystallization temperature from amorphous phase to anatase phase and accelerates the transition process from anatase phase to rutile phase [24]. From the information of TGA–DSC analysis on pure TiO₂ and Sn doped TiO₂, a temperature of 673 K was selected for the calcination of the different materials.

The X-ray diffractograms for samples with different Sn⁴⁺ concentrations, after they were heat treated at 673 K during 4 h with a heating rate of 2 K/min, are depicted in Fig. 2.

The anatase is the only crystalline phase present in the undoped TiO₂ sample (JCPDS card 21-1272). In all doped samples, even that containing 0.1% mol of Sn⁴⁺, in addition to anatase, brookite (JCPDS card 29-1360) phase is present. Upper vertical marks on the bottom correspond to anatase phase, whereas the lower ones correspond to brookite. The arrow pointing up is the characteristic Bragg reflection of brookite, whereas the asterisk corresponds to the characteristic Bragg reflection of cassiterite (SnO₂).

Since the crystallography of anatase and brookite phases are well known [26,27], these diffractograms were refined by Rietveld method (Fig. 2), to study the effect of Sn⁴⁺ on the crystal properties of both phases, including cell parameters, crystallite size and relative concentration of anatase and brookite in the doped samples. The initial values for the relative coordinates of brookite were those reported by Meagher and Lager [27]. In Table 1 are shown the lattice parameters, the crystallite size and the concentration in weight obtained from the Rietveld refinements for anatase and brookite as a function of Sn⁴⁺ content. The data in Table 1 shows

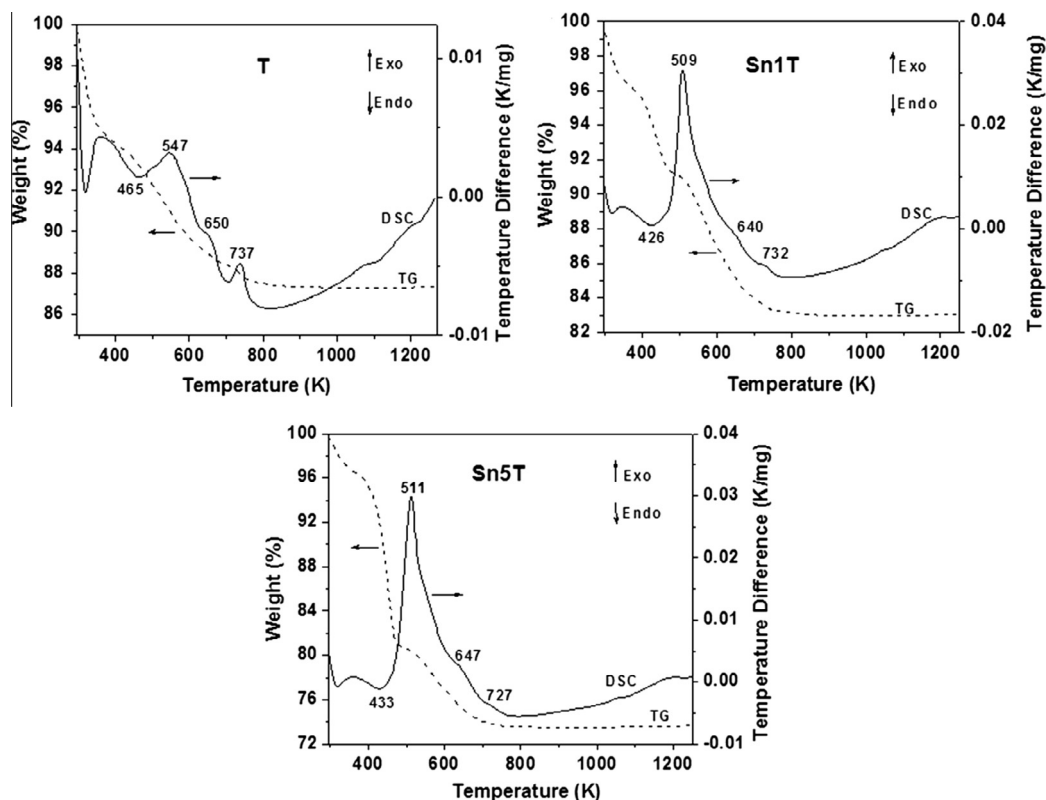


Fig. 1. TGA–DSC profiles of the thermal evolution for sol–gel samples TiO_2 (T), Sn1T, Sn5T.

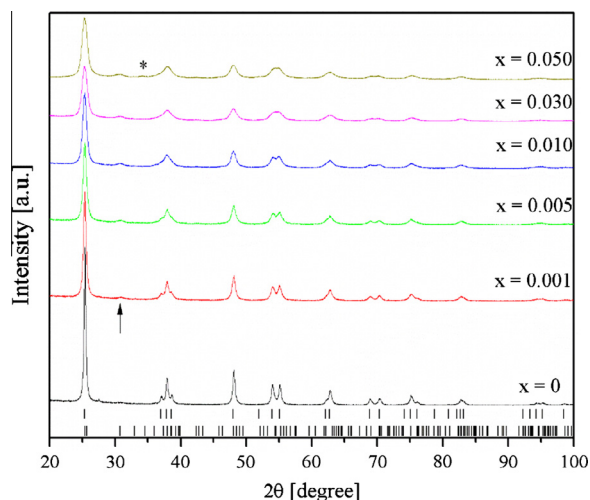


Fig. 2. X-ray diffraction patterns of TiO_2 and Sn^{4+} -doped TiO_2 photocatalysts at different mol% concentrations of Sn^{4+} , Rietveld refinement. Upper vertical marks on the bottom correspond to anatase, whereas the lower ones correspond to brookite. Asterisk corresponds to the characteristic Bragg reflection of cassiterite (SnO_2).

important facts concerning the effect of the addition of Sn^{4+} into TiO_2 . By increasing the amount of Sn^{4+} , there is a significant reduction (50% of the value compared to the undoped sample) in the crystallite size of the anatase. At the same time, it is observed an increase in the weight concentration of brookite. The diminishing in crystallite size as the Sn^{4+} concentration increases is due to the difference between the ionic radius of Ti^{4+} and that one of Sn^{4+} . In a six-coordination, like that present in anatase and brookite structures, the ionic radii of Ti^{4+} and Sn^{4+} are 0.605 and 0.69 Å, respectively [19]. This difference which is around 14% in size,

should be introducing a perturbation in the crystal structure of anatase, in a way that inhibits the growth of the crystallites. Something similar happens in brookite, because it is also observed a decrease in crystallite size with increasing Sn^{4+} concentration (Table 1). However, it seems to be a solubility limit of the Sn^{4+} ions into the TiO_2 crystal phases, since at 5 mol% appears the cassiterite phase of SnO_2 . The slightly increase observed in the cell parameter of anatase, from 3.78502(12) Å (undoped sample) to 3.7878(12) Å (sample doped with 3 mol% of Sn^{4+}), is an evidence of the incorporation of the larger Sn ion added, at least partially, into the anatase crystal cell. The analysis of the probable incorporation of Sn^{4+} into brookite crystal cell was not performed, because many Bragg reflections are overlapped with those ones of anatase. Furthermore, lower concentration phase and small crystallite size produce less intense and broad diffraction peaks. All of these factors make impossible to get a reasonable trend in the lattice parameters of brookite for any amount of Sn^{4+} added. Actually, the cell parameters of brookite were modeled as constants as those reported [27].

The effect of the incorporation of Sn^{4+} to the TiO_2 structure is the production of brookite and showing an increase in the relative weight (%) by the increase of mol% of Sn^{4+} . The reason which favors the brookite phase is the substitution of Sn^{4+} by Ti^{4+} in the different species of titanium tetrahedral [TiO_4] and titanium octahedral [TiO_6] modifying the distortion energy [28]. In the Sn5T, according to weak signal of XRD analysis for Sn^{4+} doped TiO_2 sample with 5 mol%, the most of Sn is as substitutional mode and the remainder as SnO_2 forming islands on the TiO_2 surface.

The Raman spectroscopy of the doping effect of TiO_2 with SnO_2 can be observed in Fig. 3. The Raman spectra presents well-defined vibration bands, at 143 cm^{-1} (E_g), 198 cm^{-1} (E_g), 399 cm^{-1} (B_{1g}), 518 cm^{-1} (B_{1g}) and 640 cm^{-1} (E_g), which correspond to the six fundamental vibration (E_g , B_{1g} , A_{1g}) modes consistent with spatial group $I4_1/amd$ (141) of the anatase phase [29]. In the same figure

Table 1

Lattice parameters, crystallite size and weight concentration obtained by Rietveld refinements for anatase and brookite as a function of Sn⁴⁺. Numbers in parentheses represent standard deviations.

Sample	Anatase				Brookite				
	Cell parameters (nm)		Crystallite size (nm)	Relative phase concentration wt (%)	Cell parameter (nm) ^a			Crystallite size (nm)	Relative phase concentration wt (%)
	a	c			a	b	c		
T	0.378502(12)	0.950208(35)	28.1(2)	100	–	–	–	–	–
Sn0.1T	0.378637(19)	0.949578(55)	23.5(2)	95.2(3)	0.9174	0.5449	0.5138	17.2(17)	4.8(3)
Sn0.5T	0.378628(27)	0.949274(80)	19.5(2)	92.1(4)	“	“	“	14.9(11)	7.9(4)
Sn1T	0.378660(33)	0.949151(98)	17.2(2)	90.7(4)	“	“	“	14.0(9)	9.3(4)
Sn3T	0.37878(12)	0.94884(39)	13.2(2)	89.3(3)	“	“	“	11.2(5)	10.7(3)

^a Cell parameters and relative coordinates of ions in the refinement of brookite phase were modeled as constants.

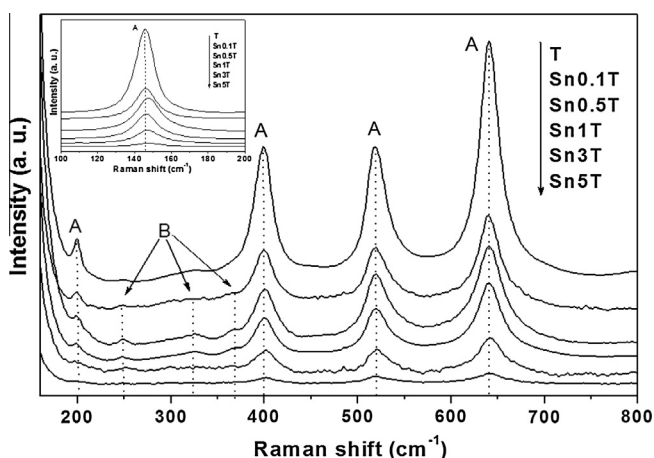


Fig. 3. Raman spectra for TiO₂ (T) and Sn doped TiO₂ samples annealed at 673 K.

other vibration modes are present at 250 cm⁻¹, 325 cm⁻¹ and 366 cm⁻¹ which are less intense, corresponding to brookite phase [30]. The Raman spectrum does not detect the main vibration bands of SnO₂ (776 cm⁻¹, 636 cm⁻¹, 547 cm⁻¹ and 490 cm⁻¹) [31]. This result can be explained by knowing that the largest amount of Sn⁴⁺ is incorporated in the TiO₂ lattice and a very small amount is present as SnO₂, which is not detected by this technique.

The adsorption–desorption isotherms of nitrogen for TiO₂–SnO₂ photocatalysts were determined. The isotherms correspond to type IV based in the IUPAC classification for mesoporous materials, with a H1 type hysteresis loop [32]. The specific surface area of tin doped TiO₂ nanomaterials obtained by BET equation is reported in Table 2. The increase of Sn⁴⁺ mol% to TiO₂, from 0.1 mol% to 5 mol% leads to an increase in specific surface area of TiO₂ which are comprised between 66 m²/g and 120 m²/g, compared with pure TiO₂ (T = 59 m²/g). These results confirm those found by XRD studies. The increase in the amount of Sn⁴⁺ into TiO₂ leads to a reduction in the crystallite size for the two phases (anatase and brookite)

conducting to an increase of the specific surface area. This is evidence that the Sn⁴⁺ plays an important role, by hindering the growth of TiO₂ particles [33]. The inhibition of the growth of anatase and brookite size could be due to the dissimilar boundaries as it has been reported [34]. Also it is observed that with the addition of Sn⁴⁺ the pore size distribution is shifted toward lower values. The mean pore diameter for the different samples goes from 34 nm for pure TiO₂ to values between 17.8 nm and 9.5 nm for samples containing concentrations from 0.1 mol% to 5 mol% of Sn⁴⁺ in TiO₂. The decrease of pore diameter goes well with the observation of the decrease in particle size with the increase of Sn⁴⁺ in TiO₂.

The TEM images as well as the particle size distribution for two selected samples, T and Sn1T are shown in Fig. 4. The average particle for T and Sn1T are 28.4 nm and 13.5 nm respectively. The nanoparticles prepared by sol gel shown similar shapes but different sizes, however it is difficult to distinguish between anatase and brookite from TEM images. The distribution of particle size for pure TiO₂ nanoparticles exhibits sizes in the range of 15–40 nm, meanwhile for Sn1T sample the distribution is around of 8 nm and 20 nm. The Sn⁴⁺ doped TiO₂ samples showed lower particles size distribution due to the presence of Sn⁴⁺, the higher the concentration of Sn⁴⁺ the lower is the particle size. These results are consistent with the XRD results.

The E_g values for the photocatalysts doped TiO₂ are in the interval of 3.20 eV and 3.16 eV compared to pure TiO₂ which has a value of 3.2 eV as shown in Table 2. The addition of different Sn⁴⁺ mol% modifies optical properties by a slight shifting toward the red region [35]. Other possible reason for the E_g shift is the presence of the brookite which is in the 3.1–3.4 eV region, and/or the decrease of the anatase and brookite particle size with the increase of Sn⁴⁺ [18,36].

The results of the effect of Sn⁴⁺ doping TiO₂ photocatalyst for the UV light 2,4-D decomposition are reported in Table 2. The 2,4-D photodecomposition follows a pseudo-first order kinetics. The conversion of 2,4-D on T, Sn1T and Sn5T photocatalysts, after 180 min, are 77%, 93% and 79% respectively. The apparent rate constant was calculated by plotting Ln (C₀/C) as a function of time (min) while the

Table 2

Specific surface area, band gap (E_g) and kinetic parameters for the degradation of 40 ppm of 2,4-dichlorophenoxyacetic acid on TiO₂ and SnO₂–TiO₂ photocatalysts.

Photocatalyst	Surface area (m ² g ⁻¹)	E _g (eV)	^a TOC %	^c K _{app} × 10 ³ (min ⁻¹)	t _{1/2} (min)	^b C %
T	59	3.22	77	9.4	73	77
Sn0.1T	66	3.20	66	8.1	85	74
Sn0.5T	75	3.18	69	7.4	93	67
Sn1T	87	3.21	81	16.8	41	93
Sn3T	106	3.19	63	8.3	83	65
Sn5T	120	3.16	70	10.5	65	79
Photolysis	–	–	20	1.7	–	29

^a TOC = Total Organic Compound at 180 minutes.

^b C% = Conversion % at 120 minutes.

^c K_{app} = Apparent constant at 120 minutes.

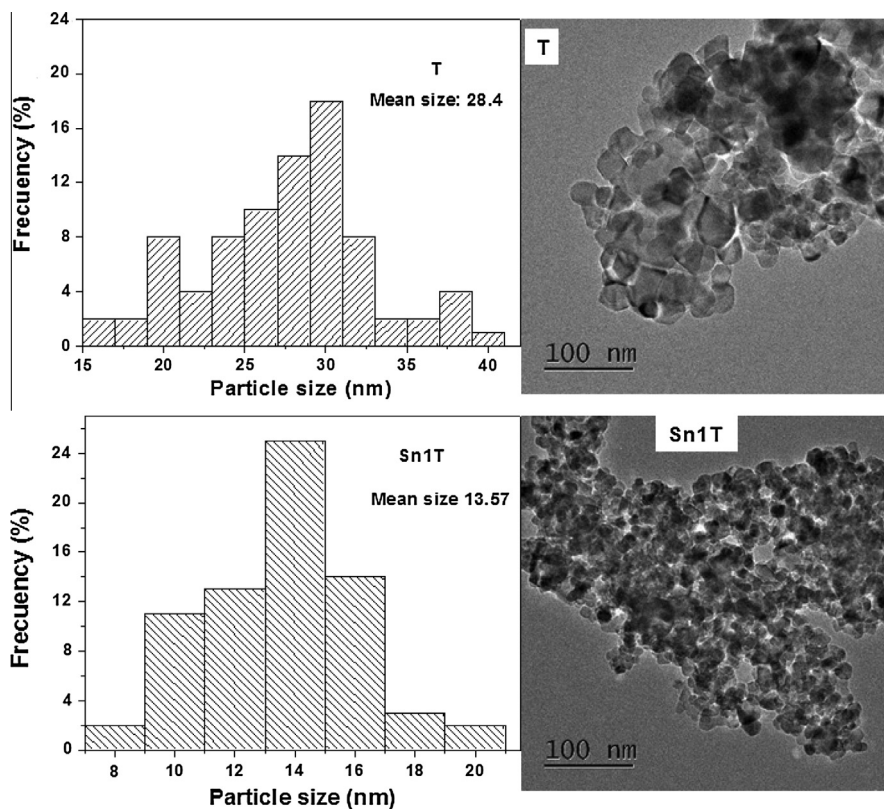


Fig. 4. The TEM images and particle size distribution measured from the micrographs for T and Sn1T samples.

values of half time life, $t_{1/2}$ (min), were determined by the $t_{1/2} = \ln 2/k$ equation. Where the C_0 and C are the concentrations (mg/L) at initial time $t(0)$ and at a given time t (min) respectively and k is the first order degradation rate constant (min^{-1}). The kinetics results reported in Table 2 shows that it exist a synergetic effect in the Sn doped TiO_2 nanoparticles for the Sn1T photocatalyst. This improvement in photocatalytic decomposition activity of 2,4-D is observed with an optimal concentration of 1 mol% of Sn^{4+} in TiO_2 . The Sn1T photocatalyst show the highest value of conversion of 93%, at the highest rate constant of $16.8 \times 10^{-3} \text{ min}^{-1}$ and the lowest half time life $t_{1/2}$ of 41 min. The total organic carbon (TOC) is 81%, corresponding to a notable elimination of the organic pollutant compound, in agreement with the above-mentioned results. The behavior of this Sn1T doped sample can be attributed to the coexistence in appropriated proportions of anatase and brookite phases of TiO_2 and with a specific particle size. Indeed, bicrystalline structure of the anatase and brookite can reduce the recombination of the photogenerated charge carrier to improve the photocatalytic activity [37]. On the other hand, the substitution of Sn^{4+} ions by Ti^{4+} ions in TiO_2 produce a distortion in the network which leads to structural defects on the surface, resulting in the presence of unsaturated surface cations [20] and surface hydroxyl groups. The unsaturated sites favor the adsorption of the organic molecule on the surface defects of $\text{TiO}_2\text{-SnO}_2$, where the molecule is oxidized by the photo-generated holes in the valence band. With the increase of the specific surface area in tin doped- TiO_2 samples, it should be expected an increase in the number of unsaturated sites and an enhancement in the photocatalytic activity. However, the activities do not go far from that showed by the Sn1T which means that a specific type of sites is required.

It was reported that Sn^{4+} incorporation leads to an increase in surface oxygen vacancies on TiO_2 , which can induce sub-band levels near the bottom of the conduction band. These sub-bands capture the photoinduced electrons and enhance the separation

of photoexcited charges resulting in an improvement in the photocatalytic activity of TiO_2 [35]. Furthermore, the hydroxyl radicals inhibit the electron-hole recombination. However, high oxygen vacancies can act as recombination centers and the photoactivity decreases [38]. This can explain the lower photoactivity for Sn3T and Sn5T samples. The higher concentration of tin in TiO_2 produces a further lattice deformation and distortion, resulting in more oxygen vacancies and decrease on the photoactivity.

4. Conclusion

Pure TiO_2 and Sn-doped TiO_2 materials were prepared by sol-gel method using titanium and tin alkoxides, varying the amounts of Sn^{4+} (0.1 mol%, 0.5 mol%, 1 mol%, 3 mol% and 5 mol%). The anatase was the only crystalline structure in the pure TiO_2 sample, whereas anatase and brookite were obtained in Sn-doped TiO_2 samples. The Sn^{4+} ion is incorporated into the crystalline structure of TiO_2 . The brookite phase increases whereas the anatase decreases with the concentration of Sn^{4+} . The Rietveld refinements method was used to determine the relative weight of anatase and brookite as a function of Sn concentration and the particle size. The presence of Sn^{4+} inhibits the growth of the particles size of anatase and brookite in TiO_2 , which leads to an increase of the specific surface area of TiO_2 . A synergetic effect in the photocatalytic activity on Sn1T photocatalyst with 1 mol% of Sn^{4+} for 2,4-D degradation reaction was observed. The maximum in activity was attributed to both the coexistence of anatase and brookite phases in the appropriate ratio and the particle size.

Acknowledgements

We acknowledge CONACYT for the support provided to the Project CB-105158 Fond SEP-CONACYT. Israel Rangel Vazquez grateful

to CONACyT for the PhD fellowship granted. The authors thank to LDRX (T-128) UAM-I for XRD measurements.

References

- [1] H.J. Kim, J.D. Jeon, D.Y. Kim, J.J. Lee, S.Y. Kwak, *J. Ind. Eng. Chem.* 18 (2012) 1807–1812.
- [2] G. Wang, Q. Wang, W. Lu, J. Li, *J. Phys. Chem. B* 110 (2006) 22029–22034.
- [3] B.K. Kaleji, *J. Sol–Gel Sci. Technol.* 67 (2013) 312–320.
- [4] Q. Wang, H. Jiang, S. Zang, J. Li, Q. Wang, *J. Alloys Comp.* 586 (2014) 411–419.
- [5] K. Sutasinee, A. Worayingyong, A. Suramitr, M.F. Smith, *Mater. Chem. Phys.* 139 (2013) 543–549.
- [6] N. Duraisamy, R.T. Rajendrakumar, *Adv. Mat. Res.* 678 (2013) 373–377.
- [7] A.S. Kumar, K.K. Nagaraja, N.M. Huang, H.S. Nagaraja, *Mater. Lett.* 123 (2014) 149–152.
- [8] D. Nassoko, Y.F. Li, J.L. Li, X. Li, Y. Yu, *Int. J. Photoenergy* 716087 (2012) 1–10.
- [9] D.R. Zhang, H.L. Liu, S.Y. Han, W.X. Piao, *J. Ind. Eng. Chem.* 19 (2013) 1838–1844.
- [10] A. Kachina, E. Puzenat, S. Ould-Chikh, C. Geantet, P. Delichere, P. Afanasiev, *Chem. Mater.* 24 (2012) 636–642.
- [11] Y.K. Lai, J.Y. Huang, H.F. Zhang, V.P. Subramaniam, Y.X. Tang, D.G. Gong, L. Sundar, L. Sun, Z. Chen, C.J. Lin, *J. Hazard. Mater.* 184 (2010) 855–863.
- [12] Y.T. Lin, C.H. Weng, Y.H. Lin, C.C. Shiesh, F.Y. Chen, *Sep. Purif. Technol.* 116 (2013) 114–123.
- [13] K. Pathakoti, S. Morrow, C. Han, M. Pelaez, X.J. He, D.D. Dionysiou, H.M. Hwang, *Environ. Sci. Technol.* 47 (2013) 9988–9996.
- [14] B. Wang, X.Y. Lu, J. Xuan, M.K.H. Leung, *Mater. Lett.* 115 (2014) 57–59.
- [15] Y.C. Wu, L.S. Ju, *J. Alloys Comp.* 604 (2014) 164–170.
- [16] E.S. Agorku, B.B. Mamba, A.C. Pandey, A.K. Mishra, *J. Nanomater.* 289150 (2014) 1–11.
- [17] C.M. Gómez, G. Del Angel, F. Tzompantzi, R. Gómez, L.M. Torres-Martínez, *J. Photochem. Photobiol. A: Chem.* 236 (2012) 21–25.
- [18] A. Kusior, J. Klich-Kafel, A. Trenczek-Zajac, K. Swierczek, M. Radecka, K. Zakrzewska, *J. Eur. Ceram. Soc.* 33 (2013) 2285–2290.
- [19] R.D. Shannon, *Acta Cryst. A32* (1976) 751–767.
- [20] Y. Cao, W. Yang, W. Zhang, G. Liu, P. Yue, *New J. Chem.* 28 (2004) 218–222.
- [21] E. Arpac, F. Sayilkan, M. Asilturk, P. Tatar, N. Kiraz, H. Sayilkan, *J. Hazard. Mater.* 140 (2007) 69–74.
- [22] G. Rangel-Porras, E. Ramos-Ramírez, L.M. Torres-Guerra, J. Porous Mater. 17 (2010) 69–78.
- [23] S. Mahanty, S. Roy, S. Sen, *J. Cryst. Growth* 261 (2004) 77–81.
- [24] Z.M. Shi, L. Yan, L.N. Jin, X.M. Lu, G. Zhao, *J. Non-Cryst. Solids* 353 (2007) 2171–2178.
- [25] L. Todan, T. Dascalescu, S. Preda, C. Andronesco, C. Munteanu, D.C. Culita, A. Rusu, R. State, M. Zaharescu, *Ceram. Int.* 40 (2014) 15693–15701.
- [26] X. Bokhimi, A. Morales, M. Aguilar, J.A. Toledo-Antonio, F. Pedraza, *Int. J. Hydrogen Energy* 26 (2001) 1279–1287.
- [27] E.P. Meagher, G.A. Lager, *Can. Mineral.* 17 (1979) 77–85.
- [28] L.H. Edelson, A.M. Glaeser, *J. Am. Ceram. Soc.* 71 (1988) 225–235.
- [29] T. Ohsaka, *J. Phys. Soc. Jpn.* 48 (1980) 1661–1668.
- [30] A. Golubovic, M. Scepanovic, A. Kremenovic, S. Askrabic, V. Berec, Z. Dohcevic-Mitrovic, Z.V. Popovic, *J. Sol–Gel Sci. Technol.* 49 (2009) 311–319.
- [31] L.C. Chen, F.R. Tsai, S.H. Fang, Y.C. Ho, *Electrochim. Acta* 54 (2009) 1304–1311.
- [32] K.S.W. Sing, D.H. Everett, R.A.W. Haul, L. Moscou, R.A. Pierotti, J. Rouquérol, T. Siemieniowska, *Pure Appl. Chem.* 57 (1985) 603–619.
- [33] M. Hirano, H. Dozono, T. Kono, *Mater. Res. Bull.* 46 (2011) 1384–1390.
- [34] J. Yu, S. Liu, M. Zhou, *J. Phys. Chem. C* 112 (2008) 2050–2057.
- [35] Y. Zhao, J. Liu, L. Shi, S. Yuan, J. Fang, Z. Wang, M. Zhang, *Appl. Catal. B Environ.* 100 (2010) 68–76.
- [36] V. Štengl, D. Králová, *Mater. Chem. Phys.* 129 (2011) 794–801.
- [37] L. Shi, D. Weng, *J. Environ. Sci.* 20 (2008) 1263–1267.
- [38] Y. Zhao, C.Z. Li, X.L. Liu, F. Gu, H.L. Du, L. Shi, *Appl. Catal. B* 79 (2008) 208–215.